Microporous and Mesoporous Materials 239 (2017) 138–146

Contents lists available at ScienceDirect

Microporous and Mesoporous Materials

journal homepage: www.elsevier.com/locate/micromeso

Chromium (VI) removal from water by means of adsorption-reduction at the surface of amino-functionalized MCM-41 sorbents

Nicolás Fellenz [a, *], Francisco J. Perez-Alonso [b], Pedro P. Martin [a], José L. García-Fierro [b], José F. Bengoa [c], Sergio G. Marchetti [c], Sergio Rojas [b]

[a] Consejo Nacional de Investigaciones Científicas y Técnicas (CONICET), Universidad Nacional de Río Negro, Av. Don Bosco y Leloir (s/n), 8500 Viedma, Río Negro, Argentina
[b] Grupo de Energía y Química Sostenibles (EQS), Instituto de Catálisis y Petroleoquímica, CSIC, C/Marie Curie, 2, L10, 28049 Madrid, Spain
[c] Departamento de Química, Facultad de Ciencias Exactas, Universidad Nacional de La Plata, CONICET, CINDECA, CICPBA, 47 No 257, 1900 La Plata, Buenos Aires, Argentina

ARTICLE INFO

Article history:
Received 1 June 2016
Received in revised form
2 August 2016
Accepted 10 October 2016
Available online 11 October 2016

Keywords:
Amino-Functionalized MCM-41
Cr(VI) removal
Adsorption
Reduction
Mesoporous sorbents

ABSTRACT

A first study that demonstrates the capability of the amino-functionalized MCM-41 sorbents to reduce Cr(VI) to the less toxic trivalent state is presented. To achieve this aim two mesoporous ordered silica with MCM-41 pores arrangement were synthesized and surface modified by a post-synthetic treatment using 3-aminopropyltriethoxysilane in toluene. The modified silicas were characterized by powder X-ray diffraction (XRD), infrared spectroscopy(FT-IR), scanning electron microscopy (SEM), nitrogen adsorption −desorption experiments, X-ray photoelectron spectroscopy (XPS), Raman spectroscopy and thermogravimetric analysis (TGA). Hexavalent chromium adsorption experiments in aqueous media were carried out with the hybrid samples at pH 2 and room temperature until reach equilibrium conditions. The experimental results showed that the aminopropyl-functionalized MCM-41 sorbents adsorb Cr(VI) and partially reduce it to the less toxic Cr(III) state. It is proposed that Cr(VI) adsorption is produced by electrostatic interaction between $HCrO_4^-$ anions and positive ammonium groups of the sorbent surface and continues with the reduction to Cr(III) while a proton is released from the solid surface to the solution. Afterwards, Cr(III) is partially retained onto the samples surface due to the Lewis basicity of the nitrogen atoms.

1. Introduction

Chromium forms part of the top-priority list of toxic inorganic pollutants defined by the US Environmental Protection Agency due to its mutagenic and carcinogenic properties against biological species [1]. Different industrial activities are associated with hazardous wastes with high contents of chromium compounds, such as alloys and steel manufacturing, metal finishing, electroplating, leather tanning, and pigments synthesis and dyeing.

In aqueous environments chromium can be found in two valence states, hexavalent (Cr(VI)) and/or trivalent (Cr(III)). Among them, hexavalent species have higher solubility and mobility in aqueous systems, and the ability to readily go thorough cell membranes. So, hexavalent chromium is reported as many times more toxic than the trivalent one [2]. Because of this, strategies for remediation of natural water resources contaminated with Cr(VI) involving a mixed mechanism of adsorption and reduction of Cr(VI) to the less toxic trivalent state, present a clear advantage versus those that only achieve separation of Cr(VI) from aqueous matrices without chemical transformation.

In this sense, a wide variety of solids have been proposed as efficient adsorbent for chromium removal from aqueous matrices. Such adsorbents are able to separate the metal from the aqueous matrix through a process based on surface interactions. Some of them, such as N-doped porous carbon, bio-based materials, natural minerals, involve a sequential adsorption of Cr(VI), in the form of $Cr_2O_7^{2-}$ or $HCrO_4^-$ onto the solid surface, and the reduction of the adsorbed Cr(VI) to the less toxic Cr(III) [3–6]. Another type of materials that have been successfully used for removal and retrieval of heavy metals are the ordered mesoporous silicas (OMS). These solids have very useful and unique properties for separation applications: high specific surface area, narrow and modulable pore

* Corresponding author.
E-mail address: nfellenz@unrn.edu.ar (N. Fellenz).

http://dx.doi.org/10.1016/j.micromeso.2016.10.012
1387-1811/

size distribution, high thermal stability and the capability to attach a wide variety of chemical (organic) functions onto its surface [7]. This last property confers to the material specificity toward the desired target pollutant [8]. Besides, the OMS substrates present other important advantages related to sustainability and environmental protection: they can be synthesized using inexpensive raw sources and they present low toxicity against biological species [9,10]. Among the OMS, the MCM-41 and SBA-15 substrates with different organics anchored groups (called organic-inorganic hybrids OMS), have been extensively studied in the separation of several aqueous inorganic pollutants such as Cu, Zn, Hg, As and Cr(VI) from water [11–14]. Due to the interest in the synthesis of long-lived and reusable adsorbents, there are many bibliographic reports dealing with the performance of hybrid OMS seeking to determine for the optimal operation conditions: pH, temperature, selectivity between different metals, contact time and regeneration procedures [12,13,15]. Remarkably, in the case of amino-functionalized OMS used for the removal of Cr(VI), there are few reports about chromium-OMS interaction and, as far as we know, no hexavalent chromium reduction to the trivalent state using amino-OMS materials has been reported.

In a previous work, we described the synthesis and characterization of a nanometer spherical aminopropyl-functionalized MCM-41 solid and reported preliminary tests results to describe its performance towards Cr(VI) adsorption from water. The synthesized nanoadsorbent showed very high capacities for chromium elimination at pH = 2 and the capability of being regenerated and reutilized several times [16].

In this work we go further and demonstrates, for the first time, that NH_2-functionalized MCM-41 sorbents are able to reduce Cr(VI) into less Cr(III) species. Besides, we discuss about the relationship between the particle size of the OMS sorbent and its capacity toward metals removal. For this purpose two different MCM-41 samples with very similar pore diameter and specific surface area but different particles sizes were synthesized and tested towards Cr(VI) adsorption after a post-synthesis modification with 3-aminopropyltriethoxysilane. X-ray photoelectron spectroscopy (XPS), Raman spectroscopy, thermogravimetric analysis (TGA) and scanning electron microscopy (SEM), among other techniques, were used to characterize the solids.

2. Experimental

2.1. Reactants

Tetraethyl orthosilicate (TEOS, 99%, Aldrich) as silica source, n-hexadecyltrimethylamonnium bromide (CTMABr,98%, Sigma) as structural directing agent, distilled water, absolute ethanol (Cicarelli, 99.5%), NH_4OH (Cicarelli, 28% p/p), 3-aminopropyltriethoxysilane (APTES, 98%, Sigma) were used. All the reactants were used as received without any further purification step.

2.2. Synthesis of MCM-41 with different particles sizes

Temperature, ratio of silica source/structural directing agent, pH, synthesis and ageing time, selected reactants and its concentrations in the synthesis gel are the operations parameters that can lead to different solids structures belonging to the OMS family [17,18]. Thus, with little variations of these parameters it is possible to obtain solids with different pore sizes, pore arrangements (e.g. hexagonal, laminar, cubic) and different particle shapes and sizes. Thus, two different synthesis procedures were selected from the literature in order to obtain MCM-41 structures with different particle sizes. The first MCM-41 substrate showing spherical morphology was synthesized by the sol–gel procedure of Grün et al., which is a variation of the Stöber synthesis of monodispersed silica spheres [19]. For this purpose, 50 mL of distilled water, 30 mL of NH_4OH, 2.5 g of CTMABr, 75 mL of absolute ethanol and 5 mL of TEOS were mixed under vigorous magnetic stirring. The synthesis gel had the following molar composition: 1 TEOS: 0.3 CTMABr: 11 NH_4OH: 58 ethanol: 144H_2O, and was kept under stirring at 30 °C for 2 h.

MCM-41 with the larger particle size was prepared according to the procedure reported by Cai et al. [20]. A mixture composed by NH_4OH (102 mL), distilled water (135 mL) and CTMABr (1.0 g) were mixed with 5.0 mL of TEOS at 30 °C and stirring during 2 h. The synthesis gel had the following molar composition: 1 TEOS: 0.125CTMABr: 69 NH_4OH: 525 H_2O.

In both cases the final white powder product was separated by filtration, washed repeatedly with water and dried in air at room temperature. Finally, to remove the CTMABr the samples were calcined up to 550 °C in air atmosphere for 3 h, with a heating rate of 10 °C min^{-1}. The final solid products are coded hereafter as s-MCM-41and l-MCM-41. The prefix denotes the particle size in the sample: s-for the solid with small particles and l-for largest particles.

2.3. Post-synthesis grafting of the materials by APTES

The aminopropyl-functionalized hybrid MCM-41 substrates were obtained by post-synthetic treatment of the s-MCM-41andl-MCM-41 samples, using 3-aminopropyltriethoxysilane (APTES, 98% Sigma) in toluene. The surface modification was realized by mixing 1 g of each calcined sample with APTES (1 mL) in toluene (100 mL) at 80 °C under vigorous stirring. After 6 h of treatment the final products were separated by filtration and repeatedly washed with ethanol and water in order to remove the non-reacted physisorbed APTES [16]. The final samples are called hereafter as s-MCM-41-NH_2 and l-MCM-41-NH_2.

2.4. Adsorption experiments

Batch-like experiments were carried out with both mesoporous aminopropyl-functionalized silica samples (s-MCM-41-NH_2 and l-MCM-41-NH_2). In a typical assay 25 mg of the selected sorbent was mixed with 25 mL of 130 ppm Cr(VI) aqueous solution. The solution pH was adjusted with HCl (8 M) to the optimal value of 2 in order to get the maximum retention capacity of the solids [16].

To reach equilibrium conditions the contact time was 24 h in all the cases [8,16,21]. After this, the solid sample was separated by filtration and stored in a dry environment until characterization. The total chromium concentration still remaining in the solution after batch assays was measured by ICP-OES. In order to discriminate between Cr (VI) and Cr (III), the presence of Cr(VI) was determined by visible–UV spectroscopy at 540 nm using the method of 1,5 diphenylcarbazide [22]. By difference between total chromium determined by ICP-OES and Cr(VI) concentration determined by visible–UV spectroscopy the amount of Cr(III) in the supernatant was calculated.

2.5. Samples characterization

The samples were subjected to several characterization techniques. The mesoporous silica structure of the hybrid samples was revealed by low angle X-ray diffraction (XRD) using a standard automated powder X-ray diffraction equipment (Philips PW 1710) provided with diffracted-beam graphite monochromator using Cu Kα radiation in the range $2\theta = 1.5°–8°$ with steps of 0.02° and counting time of 2 s.$step^{-1}$. Fourier transform infrared spectra (FT-

IR) of dried samples mixed with KBr (1:100), before and after APTES treatment, were obtained on a Jasco FT/IR-4200 spectrometer equipped with a Pike Diffuse IR cell with a resolution of 1 cm^{-1}. Two hundred to four hundred scans were accumulated in each case. The textural properties, specific surface area (Sg), specific pore volume (Vp) and pore diameter (Dp) were evaluated from the nitrogen adsorption-desorption isotherms recorded at −196 °C on samples dried overnight at 100 °C under vacuum in a Micromeritics equipment ASAP 2020 V1.02 E. The pore size distribution was determined using the Barret-Joyner-Halenda method (BJH).Thermal analysis (TGA) were performed on a ShimadzuTGA-50 apparatus, upon heating the samples from room temperature to 750 °C at a heating rate of 5 °C min^{-1}under air flow (20 mL min^{-1}). XPS spectra were acquired with a VG ESCALAB 200R spectrometer in the pulse-count mode at a pass energy of 50 eV using a MgKα (hν = 1253.6) X-ray source. Kinetic energies of photoelectrons were measured using a hemispherical electron analyzer working in the constant pass energy mode. The background pressure in the analysis chamber was kept below 7×10^{-9} mbar during data acquisition. The powder samples were pressed into copper holders and then mounted on a support rod placed in the pretreatment chamber. The XPS data were signal averaged for at least 200 scans and were taken in increments of 0.07 eV with dwell times of 40 ms. Binding energies (BEs) were calibrated relative to the C 1s peak from carbon contamination of the samples at 284.6 eV to correct for contact potential differences between the sample and the spectrometer. High-resolution spectral envelopes were obtained by curve fitting synthetic peak components using the *XPS peak* software. The raw data were used with no preliminary smoothing. Symmetric Gaussian-Lorentzian product functions were used to approximate the line shapes of the fitting components. Raman spectra of the Cr-loaded samples (samples after batch-like adsorption assays) were recorded using a single monochromator Renishaw in Via Raman Microscope System 1000 spectrometer equipped with a 100 mW laser with emission at 532 nm equipped with a thermoelectrically cooled CCD detector utilized to collect the Raman scattered radiation. The spectral range have been kept between 200 and 3100 cm^{-1} with resolution 5 cm^{-1}, accuracy 2 cm^{-1} at spectrometer slit width 100 μm.

3. Results and discussion

3.1. Samples characterization

The solids structures on the samples before and after APTES treatment were studied by XRD (Fig. 1). The X-ray diffractions patterns for all samples have an intense peak at $2\theta = 2.6°$ plus two broader and less intense peaks between $2\theta = 4$ and 6°. These diffraction patterns are characteristic of a hexagonal mesoporous arrangement, and, in our case, are indicative of the formation of MCM-41 type materials [18,20]. The X-ray diffractions patterns of the bare MCM-41 samples and the modifies ones shows no significant differences between them, thus, the APTES treatment does not generates any structural changes.

The incorporation of the aminopropyl groups to the mesoporous systems was confirmed by FT-IR (Fig. 2). The spectra of the bare MCM-41 samples display the characteristics bands at 1090 and 810 cm^{-1} which can be assigned to the antisymmetric and symmetric stretching vibration modes of the Si-O-Si species, respectively. The organically modified samples show spectra with additional bands with respect to the bare MCM-41 samples. These bands at 690 and 1560 cm^{-1} can be attributed to the presence of aminopropyl functionalities [23]. It is important to remark that the Si-OH band at 960 cm^{-1} present in the bare MCM-41 sample turns into a shoulder upon functionalization with APTES, indicating that

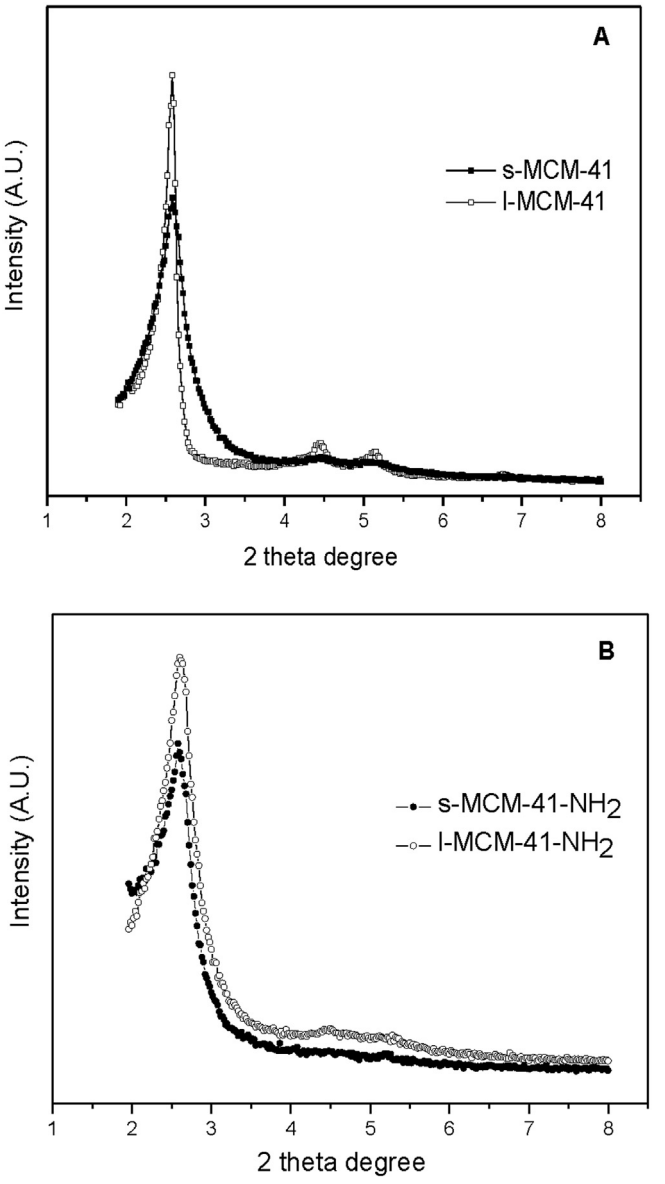

Fig. 1. Powder X-ray diffraction profiles at low angles of A: s-MCM-41(full squares) and l-MCM-41 (empty squares), B: s-MCM-41-NH_2 (full circles) and l-MCM-41-NH_2 (empty circles).

the aminopropyl groups are covalently linked and were incorporated by substituting surface silanols [23].

The nitrogen adsorption-desorption isotherms at −196 °C for the pristine MCM-41 samples and aminopropyl-modified ones are shown in Fig. 3. The textural properties of the solids before and after surface functionalization are shown in Table 1. All the isotherms are type IV according the IUPAC classification [24]. The absence of a hysteresis loop is associated with a reversible adsorption–desorption process suggesting the presence of pores with diameters smaller than 4 nm [25]; this conclusion was confirmed with the BJH average pore diameter values listed in Table 1. In the case of the organically modified samples the point corresponding to capillary condensation shifts towards lower P/P_0 values indicating a reduction in the pores size caused by the post-synthesis treatment. The initial BET surface area of both MCM-41 samples are almost the same, but the drop in this parameter after aminopropyl attachment presents a major difference. The sample l-

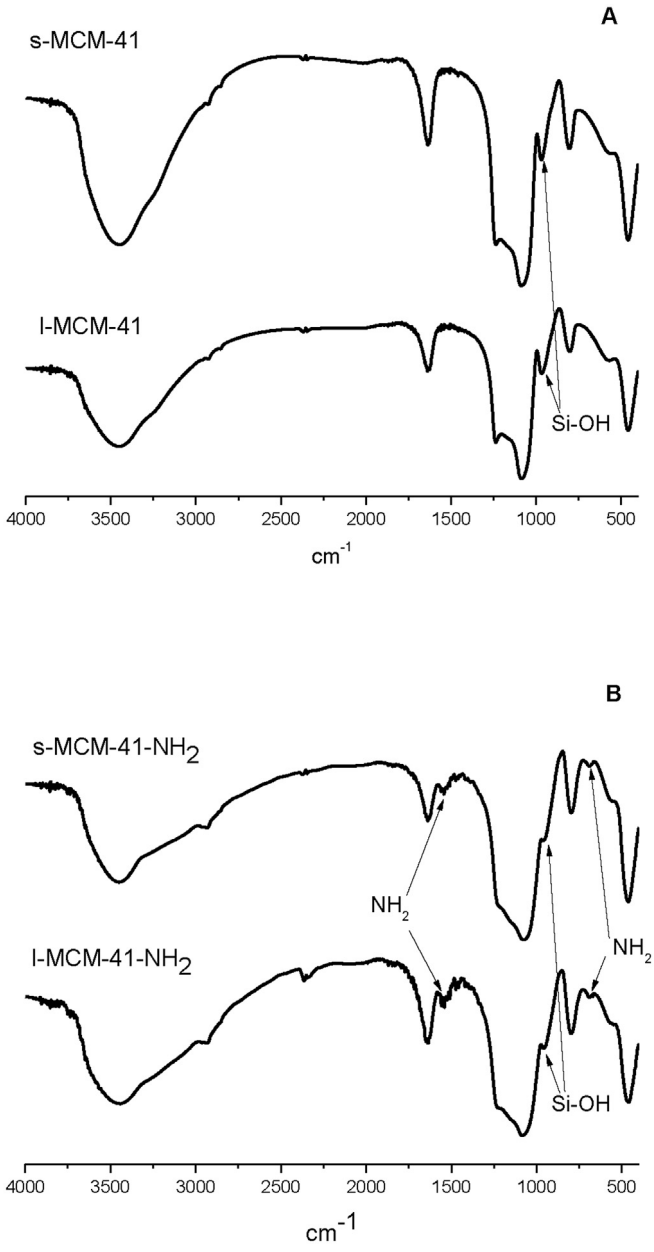

Fig. 2. FT-IR spectra of (A) bare MCM-41 samples and (B) hybrid mesoporous samples s-MCM-41-NH_2 and l-MCM-41-NH_2.

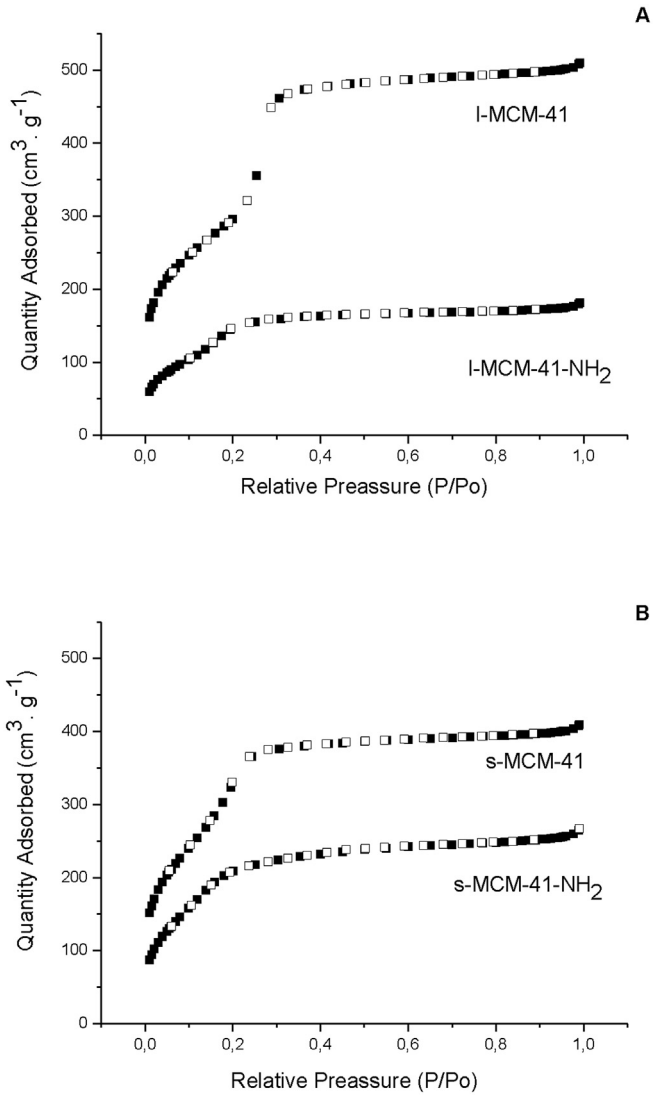

Fig. 3. Nitrogen adsorption (full symbols)-desorption (empty symbols) isotherms for pristine MCM-41 and hybrid mesoporous samples. **A**: l-MCM-41 and l-MCM-41-NH_2 couple. **B**: s-MCM-41 and s-MCM-41-NH_2 couple.

MCM 41-NH_2 shows a decrease of 18% higher than s-MCM 41-NH_2. A similar behavior was observed in the total pore volume values while the pore diameter (Dp) changes in same magnitude for both samples. The observed reduction in Dp jointly with the FT-IR spectra confirm that the aminopropyl groups are covalently attached onto the walls inside the mesopores by replacing Si-OH surface groups [21,23].

Fig. 4 shows representatives SEM images of the s-MCM-41-NH_2 and l-MCM-41-NH_2 samples and their particle size distributions obtained considering 150 particles for each sample. The distributions were fitted using a Gauss function. It can be seen that both samples are composed mostly of spherical particles. The diameter (arithmetic mean) is equal to 475 ± 11 and 866 ± 18 nm and the estimated width at half height (FWHM) is 276 and 493 nm for s-MCM-41-NH_2 and l-MCM-41-NH_2 respectively. The values obtained with the same procedure for the bare MCM-41 samples (Table 1) allow concluding that the aminopropyl incorporation does not modify the morphology of the sorbents.

In order to evaluate the penetration of APTES functionalities within the pores of the two MCM-41 structures with different particles sizes, TGA and XPS studies were conducted. TGA characterization was carried out to obtain the bulk (total) content of aminopropyl groups in the hybrid samples, whereas XPS spectroscopy was used to quantify the surface concentration of aminopropyl species. Although TGA technique is not useful to calculate the exact amount of organic groups bonded to the pore walls of the mesoporous matrices, it does allow a comparison between different samples functionalized with the same procedure like our case. Based on this assumption, the aminopropyl content (mmol per gram of sample) was 1.9 and 1.4 for s-MCM-41-NH_2 and l-MCM-41-NH_2, respectively. The nitrogen/silicon atomic ratios (N:Si) calculated from TGA and XPS measurements are listed in Table 1. The concentration of surface amino groups is almost the same for the two hybrid MCM 41 samples, but the bulk amino content is bigger (≈30%) for the MCM-41 sample with small particle size. From the differences between the N:Si ratios obtained

Table 1
Textural properties and nitrogen-silicon atomic ratios of pristine MCM-41 and the hybrid mesoporous sampless-MCM-41-NH_2 and l-MCM-41-NH_2.

Sample/ Parameter	Particles diameter (nm)[a]	Surface area ($m^2\ g^{-1}$)[b]	Pore volume ($cm^3\ g^{-1}$)[b]	Pore diameter (nm)[c]	Functional group loading (mmol g^{-1})[d]	N:Si bulk ratio[d]	N:Si surface ratio[e]
s-MCM 41	495 ± 27	1143	0.6	2.9	–	–	–
s-MCM 41-NH_2	475 ± 11	774	0.4	2.5	1.9	0.12 ± 0.01	0.16 ± 0.01
l-MCM 41	846 ± 28	1055	0.7	3.0	–	–	–
l-MCM 41-NH_2	866 ± 18	517	0.3	2.4	1.4	0.09 ± 0.01	0.14 ± 0.01

[a] By SEM.
[b] By nitrogen sorption (BET).
[c] BJH method.
[d] By TGA analysis.
[e] By XPS measurements.

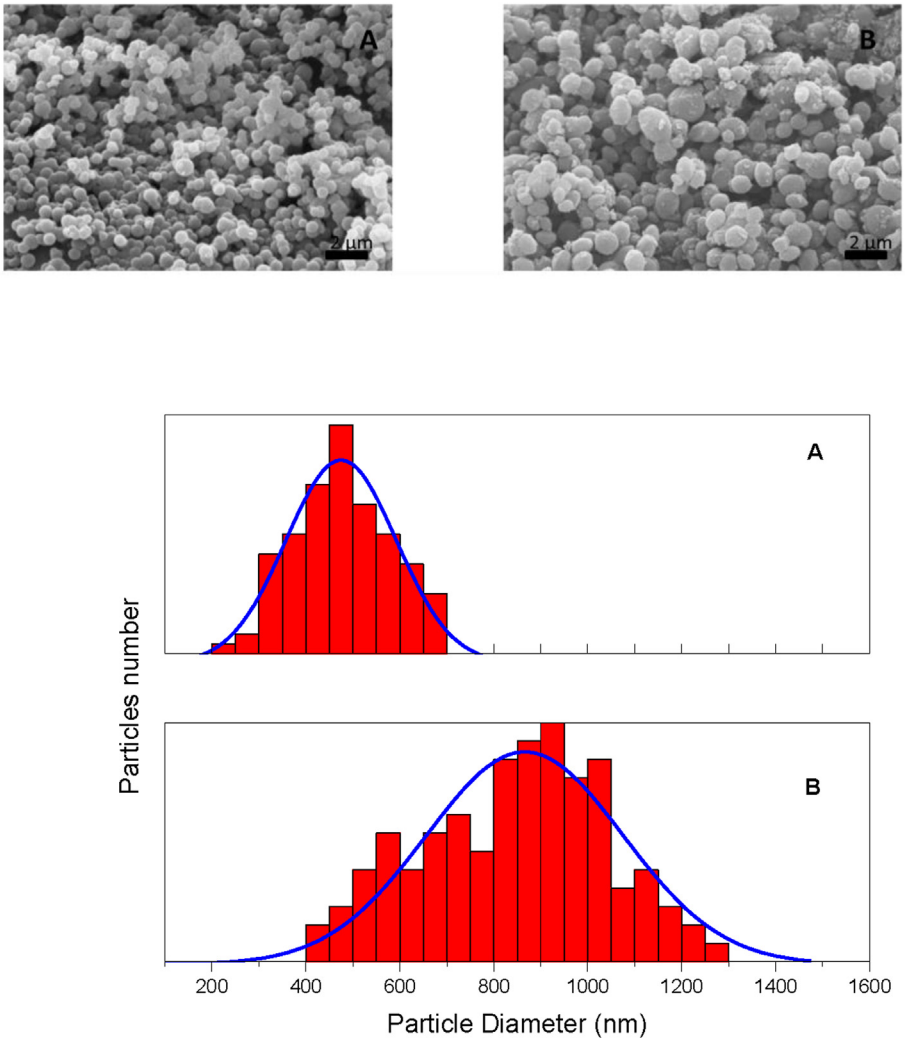

Fig. 4. SEM images and particle sizes distribution of s-MCM-41-NH_2 (A) and l-MCM-41-NH_2 (B) obtained from SEM measurements (blue lines: fitting by assuming Gaussian distribution). The bar scale corresponds to 2 µm. (For interpretation of the references to colour in this figure legend, the reader is referred to the web version of this article.)

from TGA and XPS it can be seen that the aminopropyl concentration is more homogeneous in the MCM-41 sample displaying the smallest particles (s-MCM-41-NH_2). On the contrary, in l-MCM-41-NH_2 the amino concentration clearly is larger on the particle surface than in the inner of the pores.

To understand the difference in the aminopropyl groups distribution over the particles in s-MCM-41-$NH_2$and l-MCM-41-NH_2samples it is necessary to keep in mind its different particle sizes and the APTES behavior during the surface modification reaction. APTES reacts with the silanols present at the surface of OMS materials, as it was demonstrated by FT-IR. This reaction is affected by temperature, reactant concentration, time, solvent type and water availability [26]. The selected values of these parameters to carry out the reaction can promote to a greater or lesser extent the formation of clusters of APTES molecules and thus, the subsequent pore blocking [27,28].When the particle size of the solid to be treated with APTES is reduced, implying shorter pores in the 2D MCM-41 pore arrangement, an increase in the organic functions

penetration is achieved, as it was demonstrated with the N:Si ratios calculated by TGA and XPS measurements (Table 1). But when particles with longer pores, as a result of a larger particle diameter in a 2D structure, are used in the functionalization reaction, a greater proportion of the initial specific surface of the pristine material remains without to functionalize. Although two samples are not enough to establish a strong tendency between particles size and APTES pore penetration, this explanation helps to understand the differences listed in Table 1 in specific surface area and total pore volume variations as a consequence of the APTES treatment.

On the other hand, the recorded variation in the surface area for s-MCM-41 due to APTES treatment is very similar to that reported by Larsen et al. for MCM-41 particles of ≈300 nm [29].They reported a decreasing from 1032 to 727 $m^2\ g^{-1}$ after APTES functionalization, and an elemental mapping realized through transmission electron microscopy-energy dispersive spectroscopy allows them to demonstrate a uniformly aminopropyl functional groups distribution over the entire particle. In our case, the variation in the specific surface area for the smallest particles system was from 1143 to 774 $m^2\ g^{-1}$, with1.9 mmol g^{-1} of functional groups loading vs1.8 mmol g^{-1} in the Larsen's system. Due to the similarity between the reported data, we can assume that in the s-MCM-41-NH_2 sample exist an uniformly aminopropyl distribution over the entire particle whereas in the sample l-MCM-41-$NH_2$the APTES functionalization only reaches the outer part of the pores. Thus, a decreasing of the particle size would produce a more efficient use of the initial specific surface area of the parent material, and it is a pathway to avoid the early pores blockage due to APTES polymerization.

3.2. Cr(VI) adsorption on s-MCM-41-NH_2 and l-MCM-41-NH_2

The total chromium, Cr(VI) and Cr(III) concentration in the supernatant resulting after batch experiments under the conditions described above calculated by a combination of ICP-OES and UV–vis spectroscopy techniques are listed in Table 2. It can be seen that the s-MCM-41-NH_2 sample presents 1.4 times higher hexavalent chromium elimination capacity from the initial aqueous solution than l-MCM-41-NH_2, 86.4 vs 63.3 mg g^{-1}. The maximum Cr(VI) elimination capacity is defined as the capability of the sorbent to decrease the initial hexavalent chromium concentration from the aqueous phase, and it was calculated taking into account the initial Cr(VI) concentration, 130 ppm in both cases, and the residual Cr(VI) concentration results obtained by UV–vis spectroscopy in the supernatant. The total chromium removal capacity for each sample, defined as the hexavalent plus trivalent chromium adsorbed onto the sorbents surface, is reported in Table 2 as Cr removal. This efficiency parameter is ≈ 1.3 times higher for the hybrid mesoporous material composed for the smallest particles. These results can be explained taking into account the textural properties differences between the two sorbents as it was discussed in the previous section (e.g., greater amount of surface functional groups per gram of solid).

Taking into account the Cr^{3+}/Cr^{6+} ratio inside the mesopores (the speciation of chromium over the solids surface will be discussed in the next section) and the chromium concentrations measured by ICP-OES and UV–Vis, the Cr(VI) reduction capacity of the samples was calculated (Table 2). Considering that the initial Cr(III) concentration is equal to cero, this parameter is defined as the total mg of Cr(III) per gram of sorbent after bath experiments: milligrams of Cr(III) in the supernatant plus the present onto the sorbents surface. The sample s-MCM-41-NH_2 shows greater ability per gram to reduce, adsorb and eliminate hexavalent chromium from an aqueous matrix than the sample l-MCM-41-NH_2. Besides, the maximum Cr(VI) elimination capacity of 86.4 mg g^{-1}, is higher than that reported for other sorbents such as modified activated carbons or bio-based sorbents [3,5].

It is worthy to remark that MCM-41 solids with attached amino functional groups studied in this work show capability for Cr(VI) reduction to the less toxic Cr(III) species which was ruled out by others authors working with similar MCM-41 systems [30–32].

3.3. XPS and Raman experiments

It is well established that the pH plays an important role in the reduction process of Cr(VI) to Cr(III), which is favoured when pH is low due to variation of the apparent potentials for Cr(VI)/Cr(III) redox couple [33]. Thus, this process has been reported for other sorbents such as bio-based sorbents, carbon based solids, minerals clays, iron magnetic compounds and silica materials with thiol/sulfonic functionalities at pH values between 2 and 4 [3,6,34,35]. One possible mechanism for the Cr(VI) adsorption-transformation at low pH values can be described as follows: firstly chromium anions interact with the sorbent positively-charged surface and, once the reduction occurs the Cr(III) species can remain adsorbed or not on the solid surface. This mechanism was called as “indirect reduction mechanism” by Park et al. for the sorption of Cr(VI) by biomaterials [36], but it was also used to describe this process for inorganic sorbents [37]. However, as it was already mentioned, there is no reports about Cr(VI) interaction with OMS amino-functionalized materials that include the mentioned redox process. Thus, with the aim to understand better the chemical processes which controls the adsorption of Cr(VI) in amino-modified MCM-41 materials, XPS and Raman experiments were carried out on the solids phases s-MCM-41-NH_2 and l-MCM-41-NH_2chromium-adsorbed (samples after batch adsorption experiments).

Fig. 5 shows the Cr2pcore-level XPS spectra of the chromium-adsorbed samples. The spectra present two asymmetric peaks assigned to the Cr2p $_{1/2}$ and Cr2p $_{3/2}$ orbitals [35]. The $Cr_{2p\ 3/2}$ component were fitted with two symmetric peaks using Lorentzian-Gaussian functions. The peak centred at 577.9 eV can be assigned to Cr(III) species while the component at 580.1 eV is attributed to Cr(VI) [38]. The ratio between the chromium species (Cr^{3+}/Cr^{6+}) calculated from the areas of the Lorentzian-Gaussian curves resulting from the fitting process of the Cr2p $_{3/2}$ component are roughly equal to 1 for both samples(Table 3).

Table 2
[1]Chromium concentrations in the supernatant (ppm) after batch adsorption experiments and [2]sorption efficiency parameters (mg g^{-1}).

	Total Cr[1]	Cr(VI)[1]	Cr(III)[1]	Cr removal[2,a]	Cr(VI) elimination[2,b]	Cr(VI) reduction[2,c]
s-MCM-41-NH_2	79.2	43.6	35.6	50.8	86.4	61.0
l-MCM-41-NH_2	92.3	66.3	26.0	37.7	63.7	44.9

All parameters are expressed per gram of sample.
[a] (milligrams of Cr(III) + milligrams of Cr(VI)) adsorbed onto the solid surface.
[b] ($Cr(VI)_{\text{initial concentration}} - Cr(VI)_{\text{final concentration}}$).
[c] ($Cr(III)_{\text{in the supernatant}} + Cr(III)_{\text{onto the solid surface}}$).

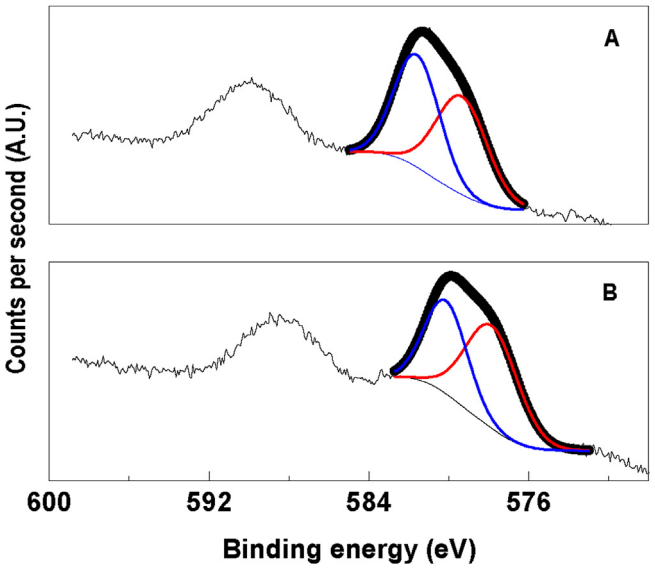

Fig. 5. Cr2p core-level XPS spectra of the chromium-adsorbed samples after batch-like experiments at pH 2 and 25 °C and fitting of the Cr2p $_{3/2}$ core-level spectrum. A: s-MCM-41-NH_2 and B: l-MCM-41-NH_2.

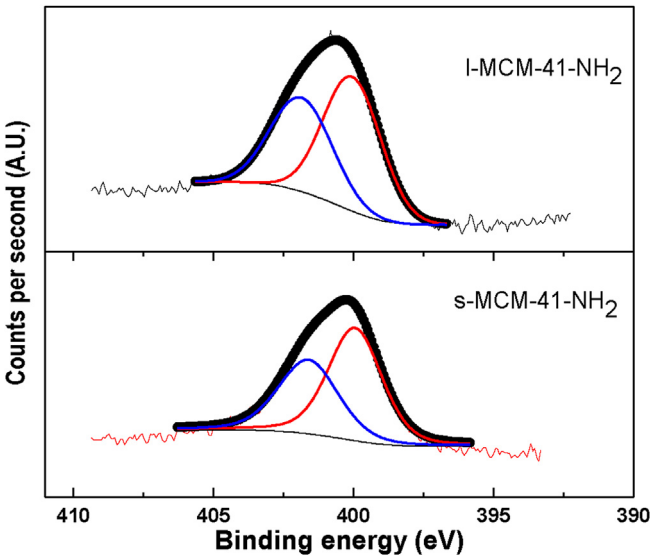

Fig. 6. N1s core-level spectra of the chromium-adsorbed samples after batch-like experiments at pH 2 and 25 °C.

The batch-like adsorptions experiments were carried out at a constant pH value of 2 and room temperature (25 °C). At this conditions, and taking into account that the pK_a of aminopropyl functionalities is in the pH range of 9–10, the surface of the aminopropyl-grafted MCM-41 samples are composed mainly of ammonium and silanols moieties, given a positively charged surface [39,40]. Thus, the XPS results shown in Fig. 5 suggests that Cr(VI) adsorption starts with anion hexavalent chromium, mainly in the form of $HCrO_4^-$, electrostatic interaction with the positive ammonium groups of the solid surface, and continues with the reduction to Cr(III). After that and according the values listed in Table 2, the trivalent chromium species are partially released back to the solution. Since at the working pH Cr(III) is mainly as $Cr(H_2O)_6^{3+}$repulsive forces adsorbate-adsorbent are expected due to the positive net surface charge in the solids [41]. Thus, it could be expected that the samples have low or non-ability to adsorb Cr(III). However, the Cr2p region of XPS spectra of the chromium-adsorbed samples displays almost the same quantities of hexavalent and trivalent chromium adsorbed onto its surfaces (Table 3 and Fig. 5).

Rivera-Utrilla*et al.* found that a positively charged surface can retain cations, specifically they explained the adsorption of cationic Cr(III) species onto a positively carbon solid surface by Cπ−cation interactions [42].To deepen the understanding of the process of chromium (VI) adsorption-reduction in the case of MCM-41 amino-grafted sorbents, it is necessary analysing changes in the solid surface due to the chromium interaction. For this purpose XPS spectra of the chromium loaded samples in the region of N1s energy were also analyzed (Fig. 6). The spectra were fitted using two Lorentzian-Gaussian components at binding energies of ≈400 and ≈ 402 eV. These components can be assigned to ammonium (-NH_3^+ at 402 eV) and amino (-NH_2 at 400 eV) species in agreement with reported values [43]. Surprisingly, the quantities of the amino groups are higher than the ammonium (Table 3). This is the opposite as the expected solid surface composition at pH = 2, where ammonium should be predominant species instead of amine [40]. As it was mentioned before, the Cr(VI) adsorption process starts with the electrostatic interaction between $HCrO_4^-$ and the positive ammonium surface species, after that, the reduction of Cr(VI) to Cr(III) occurs while a proton of the ammonium group is released from the solid surface to the aqueous medium. At this moment an amino species is generated and the Lewis basicity of the nitrogen atom acts in order to retain the positive chromium species. This assumption is in accordance with the data listed in Table 3, the relative areas of Cr(III)/Cr(VI) are almost the same that the ammonium/amine ratios for both samples. On the other hand, we cannot discard that the remnants silanols on the solid surface contribute in some extend to retain the Cr(III) species.

In order to corroborate with another technique the presence of different chromium oxidation states at the samples surface, Raman spectroscopy experiments were carried out on the samples after the adsorption assays (Fig. 7). The spectra are dominated by a broad and intense band around 860 cm^{-1} that is ascribed to Cr=O stretching vibration of chromate species [44]. This in agreement with previously reported Raman data for low-loaded chromium oxide catalysts and essentially corresponds to a sub-monolayer adsorption of chromate species onto both amine-functionalized MCM-41 samples. In addition, the presence of a broad band at 500 cm^{-1} is a clear indication of the presence of (Cr(III)-O. species) [45]in good accordance with the XPS results. Remarkably both samples present the same spectra after Cr adsorption. This is a confirmation that, in spite of their different particle size, both samples present similar surface chemical properties.

Table 3
Ratios species onto chromium-adsorbed samples surfaces calculated by XPS after bath-like assays.

	Cr(III)/Cr(VI)	-NH_2/-NH_3^+
s-MCM-41-NH_2	1.4	1.4
l-MCM-41-NH_2	1.2	1.3

4. Conclusions

Two MCM-41 sorbents with different particles sizes but very similar pore diameters were synthesised and their surface were functionalized with aminopropyl groups. According to TGA and XPS

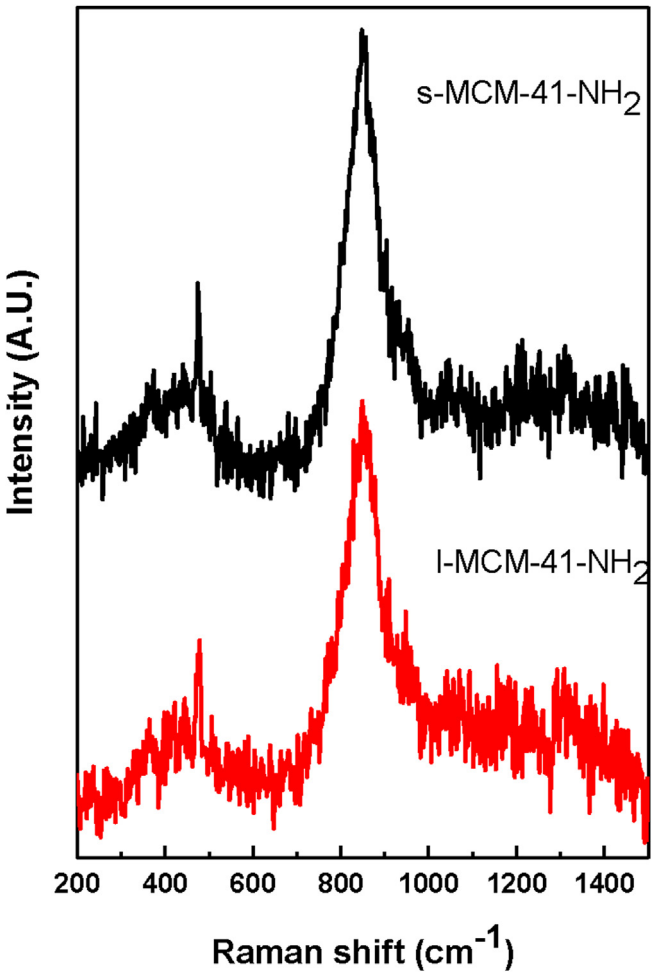

Fig. 7. Raman spectra of the chromium-adsorbed samples after bath-like assays at pH 2 and 25 °C s-MCM-41-NH_2 (black) and l-MCM-41-NH_2 (red). (For interpretation of the references to colour in this figure legend, the reader is referred to the web version of this article.)

results, the aminopropyl-functionalized MCM-41 sample composed by the smallest particles showed more uniform distribution functional groups over the entire particle. On the other hand, the sample with bigger particle size shows an enrichment of aminopropyl functionalities on the external surface of the particles.Both amino-functionalized MCM-41 sorbents showed high efficiency for aqueous Cr(VI) elimination at pH 2, although the sample with smaller particle size showed higher Cr(VI) elimination capacity, 86.4 vs 63.3 mg g^{-1}. This study shows, for the first time, that the final Cr(VI) concentration, when NH_2-MCM-41 are used, decreases dramatically after batch-like assays in acidic conditions throughout a mixed adsorption-reduction process. The adsorption of hexavalent chromium starts with the electrostatic interaction between $HCrO_4^-$ and the positive ammonium surface species. Later, according to the XPS spectroscopy experiments, a partial reduction to Cr(III) occurs while a proton is released from the solid surface. The Cr(III) was partially retained onto the samples surface due to the Lewis basicity of the nitrogen atoms of amino anchored groups, given an atoms ratio Cr^{3+} to Cr^{6+}roughly equal to 1 over the samples. This finding demonstrates that the amino-functionalized MCM-41 sorbents present an advantage versus those who only achieve separation of Cr(VI) from aqueous matrices without chemical transformation due to the Cr(III) less toxicity against biological species.

Acknowledgments

This work was funded by Universidad Nacional de Río Negro (UNRN) (PI-40-C-392) and Secretaría de Políticas Universitarias (SPU). PPM thanks Consejo Nacional de Investigaciones Científicas y Técnicas (CONICET) for his graduate student fellowship. Authors would like to thank Dr. Miguel A. Peña-Jimenez for his valuable assistance in TGA measurements and to Lic. Pablo Fetsis for his assistance with the nitrogen sorption experiments. NAF is deeply grateful to all the staff of the Instituto de Catálisis y Petroleoquímca for their great assistance and support during his stay in the institute.

References

[1] V. Bianchi, A. Zantedeschi, A. Montaldi, F. Majone, Trivalent chromium is neither cytotoxic nor mutagenic in permealized hamster fibroblasts, Toxicol. Lett. 23 (1984) 51–59.
[2] M. Baikousi, A.B. Bourlinos, A. Douvalis, T. Bakas, D.F. Anagnostopoulos, J. Tuček, K. Šafářova, R. Zboril, M.A. Karakassides, Synthesis and characterization of γ-Fe_2O_3/carbon hybrids and their application in removal of hexavalent chromium ions from aqueous solutions, Langmuir 28 (2012) 3918–3930.
[3] Y. Li, S. Zhu, Q. Liu, Z. Chen, J. Gu, C. Zhu, T. Lu, D. Zhang, J. Ma, N-doped porous carbon with magnetic particles formed in situ for enhanced Cr(VI) removal, Water Res. 47 (2013) 4188–4197.
[4] D. Park, Y.-S. Yun, J.M. Park, XAS and XPS studies on chromium-binding groups of biomaterial during Cr(VI) biosorption, J. Coll. Interf. Sc. 317 (2008) 54–61.
[5] G. Cimino, A. Passerini, G. Toscano, Removal of toxic cations and Cr(VI) from aqueous solutions by Hazelnut shell, Water Res. 34 (2000) 2955–2962.
[6] P. Misaelides, Application of natural zeolites in environmental remediation: a short review, Micro. Meso. Mater. 144 (2011) 15–18.
[7] I.I. Slowing, J.L. Vivero-Escoto, B.G. Trewyn, V.S. Lin, Mesoporous silica nanoparticles: structural design and applications, J. Mater. Chem. 20 (2010) 7924–7937.
[8] N.A. Fellenz, I.O. Pérez De Berti, A.L. Soldati, S.J. Stewart, S.G. Marchetti, J.F. Bengo, Changes on structural and magnetic properties of maghemite nanoparticles during their coverage with MCM-41, Ceram. Inter. 41 (2015) 15057–15066.
[9] S. Chiarakorn, T. Areeroba, N. Grisdanurak, Influence of functional silanes on hydrophobicity of MCM-41 synthesized from rice husk, Sci. Tech. Adv. Mater. 8 (2007) 110–115.
[10] T. Liu, L. Li, X. Teng, X. Huang, H. Liu, D. Chen, J. Ren, J. He, F. Tang, Single and repeated dose toxicity of mesoporous hollow silica nanoparticles in intravenously exposed mice, Biomaterials 32 (2011) 1657–1668.
[11] H. Yoshitaque, Design of functionalization and structural analysis of organically-modified siliceous oxides with periodic structures for the development of sorbents for hazardous substances, J. Mater. Chem. 20 (2010) 4537–4550.
[12] D. Pérez-Quintanilla, I. Sierra, Factors affecting Hg(II) adsorption on hybrid nanostructured silicas: influence of the synthesis conditions, J. Porous Mater. 21 (2014) 71–80.
[13] A. Walcarius, L. Mercier, Mesoporous organosilica adsorbents: nano-engineered materials for removal of organic and inorganic pollutants, J. Mater. Chem. 20 (2010) 4478–4511.
[14] V. Hernández-Morales, R. Nava, Y.J. Acosta-Silva, S.A. Macías-Sánchez, J.J. Pérez-Bueno, B. Pawelec, Adsorption of lead (II) on SBA-15 mesoporous molecular sieve functionalized with $-NH_2$ groups, Micro. Meso. Mater. 60 (2012) 133–142.
[15] R. Saad, K. Belkacemi, S.H. Saha, Adsorption of phosphate and nitrate anions on ammonium-functionalized MCM-48: effects of experimental conditions, J. Coll. Interf. Sc. 311 (2007) 375–381.
[16] N.A. Fellenz, P.P. Martin, S.G. Marchetti, J.F. Bengoa, Aminopropyl-modified mesoporous silica nanospheres for the adsorption of Cr(VI) from water, J. Porous Mat. 22 (2015) 729–738.
[17] A. Firouzi, D. Kumar, L.M. Bull, T. Besier, P. Sieger, Q. Huo, S.A. Walker, J.A. Zasadzinski, C. Glinka, J. Nicol, Science 267 (1995) 138–1143.
[18] R. Ryoo, J.M. Kim, Structural order in MCM-41 controlled by shifting silicate polymerization equilibrium, J. Chem. Soc. Chem. Commun. (1995) 711–712.
[19] M. Grün, K.K. Unger, A. Matsumoto, K. Tsutsumi, Novel pathways for the preparation of mesoporous MCM-41 materials: control of porosity and morphology, Micro. Meso. Mater. 27 (1999) 207–216.
[20] Q. Cai, W.-Y. Lin, F.-S. Xiao, W.-Q. Pang, X.-H. Chen, B.-S. Zou, The preparation of highly ordered MCM-41 with extremely low surfactant concentration, Micro. Meso. Mater. 32 (1999) 1–15.

[21] J. Cao, Y. Wub, Y. Jin, P. Yilihan, W. Huang, Response surface methodology approach for optimization of the removal of chromium(VI) by NH_2-MCM-41, J. Taiwan Inst. Chem. Eng. 45 (2014) 860–868.
[22] APHA, Standard Methods for the Examination of Water and Wastewater, sixteenth ed., 1985. Washington, DC.
[23] M.V. Lombardo, M. Videla, A. Calvo, F.G. Requejo, G.J.A.A. Soler-Illia, Amino-propyl-modified mesoporous silica SBA-15 as recovery agents of Cu(II)-sulfate solutions: adsorption efficiency, functional stability and reusability aspects, J. Hazard. Mater. 223– (224) (2012) 53–62.
[24] P.E. Balbuena, K.E. Gubbins, Theoretical interpretation of adsorption behavior of simple fluids in slit pores, Langmuir 9 (1993) 1801–1814.
[25] J. Villarroel Rocha, D. Barrera, K. Sapag, Improvement in the pore size distribution for ordered mesoporous materials with cylindrical and spherical pores using the kelvin equation, Top. Catal. 54 (2011) 121–134.
[26] J. Kim, P. Seidler, L.S. Wan, C. Fill, Formation, structure, and reactivity of amino-terminated organic films on silicon substrates, J. Coll. Interf. Sc. 329 (2009) 114–119.
[27] J.A. Howarter, J.P. Youngblood, Optimization of silica silanization by 3-Aminopropyltriethoxysilane, Langmuir 22 (2006) 11142–11147.
[28] N. Gartmann, C. Schütze, H. Ritter, D. Brühwiler, The effect of water on the functionalization of mesoporous silica with 3-Aminopropyltriethoxysilane, J. Phys. Chem. Lett. 1 (2010) 379–382.
[29] S. Egodawatte, A. Datt, E.A. Burns, S.C. Larsen, Chemical insight into the adsorption of chromium(III) on iron oxide/mesoporous silica nanocomposites, Langmuir 31 (2015) 7553–7562.
[30] S.A. Idris, K. Alotaibi, T.A. Peshkur, P. Anderson, L.T. Gibson, Preconcentration and selective extraction of chromium species in water samples using amino modified mesoporous silica, J. Coll. Interf. Sc. 386 (2012) 344–349.
[31] S.A. Idris, K.M. Alotaibi, T.A. Peshkur, P. Anderson, M. Morris, L.T. Gibson, Adsorption kinetic study: effect of adsorbent pore size distribution on the rate of Cr (VI) uptake, Micro. Meso. Mater. 165 (2013) 99–105.
[32] A. Benhamou, J.P. Basly, M. Baudu, Z. Derriche, R. Hamacha, Amino-functionalized MCM-41 and MCM-48 for the removal of chromate and arsenate, J. Coll. Interf. Sc. 404 (2013) 135–139.
[33] J.W. Ball, D.K. Nordstrom, Critical evaluation and selection of standard state thermodynamic properties for chromium metal and its aqueous ions, hydrolysis species, oxides, and hydroxides, J. Chem. Eng. Data 43 (1998) 895–918.
[34] N. Zaitseva, V. Zaitsev, A. Walcarius, Chromium(VI) removal via reduction–sorption on bi-functional silica adsorbents, J. Hazard. Mater. (2013), 250– 251, 454– 461.
[35] Y. Liu, Y. Wang, S. Zhou, S. Lou, L. Yuan, T. Gao, X. Wu, X. Shi, K. Wang, Synthesis of high saturation magnetization superparamagnetic Fe_3O_4 hollow microspheres for swift chromium removal, Appl. Mater. Interfaces 4 (2012) 4913–4920.
[36] D. Park, Y.-S. Yun, J.M. Park, Studies on hexavalent chromium biosorption by chemically-treated biomass of Ecklonia sp, Chemosphere 60 (2005) 1356–1364.
[37] D. Mohan, C.H. Pittman Jr., Review: activated carbons and low cost adsorbents for remediation of tri- and hexavalent chromium from water, J. Hazard. Mater. 137 (2006) 762–811.
[38] S.R. Chowdhurya, E.K. Yanful, A.R. Pratt, Chemical states in XPS and Raman analysis during removal of Cr(VI) from contaminated water by mixed maghemite–magnetite nanoparticles, J. Hazard. Mater. (2012), 235– 236, 246– 256.
[39] J.M. Rosenholm, M. Lindén, Wet-chemical analysis of surface concentration of accessible groups on different amino-functionalized mesoporous SBA-15, Chem. Mater. 19 (2007) 5023–5034.
[40] M. Etienne, A. Walcarius, Analytical investigation of the chemical reactivity and stability of aminopropyl-grafted silica in aqueous medium, Talanta 59 (2003) 1173–1188.
[41] S.A. Idrees, K. Alotaibi, T.A. Peshkur, P. Anderson, L.T. Gibson, Preconcentration and selective extraction of chromium species in water samples using amino modified mesoporous silica, J. Phys. Chem. C 116 (2012) 3517–3523.
[42] J. Rivera-Utrilla, M. Sánchez-Polo, Adsorption of Cr(III) on ozonised activated carbon. Importance of Cπ—cation interactions, Water Res. 37 (2003) 3335–3340.
[43] A. Calvo, P.C. Angelome, V.M. Sanchez, D.A. Scherlis, F.J. Williams, G.J.A.A. Soler-Illia, Mesoporous aminopropyl-functionalized hybrid thin films with modulable surface and environment-responsive behavior, Chem. Mater. 20 (2008) 4661–4668.
[44] M.A. Vuurman, D.J. Stufkens, A. Oskam, J.A. Moulijn, F. Kapteijn, Raman spectra of chromium oxide species in CrO_3/Al_2O_3 catalysts, J. Mol. Catal. 60 (1990) 83–98.
[45] R.L. McCreery, Raman Spectroscopy for Chemical Analysis, Wiley, New York, 2000, pp. 15–30.